

# 稀土氧化物掺杂对 SnO<sub>2</sub> 基气体传感器 材料性能的影响

李来风<sup>1,2</sup> 潘晓晴<sup>2</sup>

(1. 中国科学院低温技术实验中心 2. 美国密西根大学)

**摘 要** 采用化学共沉淀法制备 Y<sub>2</sub>O<sub>3</sub>, ZrO<sub>2</sub>, Er<sub>2</sub>O<sub>3</sub> 和 Sb<sub>2</sub>O<sub>3</sub> 掺杂 SnO<sub>2</sub> 基气体传感器. 结果表明掺杂后的材料经煅烧后, 平均晶粒尺寸均小于 30nm, 比未经掺杂的材料小. 将各掺杂体系不同成分材料制备成厚膜传感器, 进行了对 CO 气体敏感度性能测试, 发现掺杂稀土氧化物的气体敏感度较纯 SnO<sub>2</sub> 厚膜传感器高. 其中掺杂 Er<sub>2</sub>O<sub>3</sub> 材料性能最好.

**关键词** 稀土氧化物 纳米 传感器

**分类号** TB381

**文章编号** 1005-3093(2000)01-0042-05

## ROLE OF ADDITIVES IN SnO<sub>2</sub> BASED GAS SENSOR MATERIALS

LI Laifeng<sup>1,2\*</sup> PAN Xiaoqing<sup>2</sup>

(1. Cryogenic Laboratory, The Chinese Academy of Sciences, Beijing 100080

2. University of Michigan, Ann Arbor, MI 48109-2136)

**ABSTRACT** Nanocrystalline SnO<sub>2</sub> powders doped with different metal oxides including Y<sub>2</sub>O<sub>3</sub>, ZrO<sub>2</sub>, Er<sub>2</sub>O<sub>3</sub> and Sb<sub>2</sub>O<sub>3</sub> were synthesized by chemical co-precipitation method. The Y, Er and Zr-SnO<sub>2</sub> are new systems and have not been reported before. The influence of dopants on the crystallite size and electrical properties has been characterized. The results showed that SnO<sub>2</sub> powders doped with 3% ~5% (mass fraction) Y<sub>2</sub>O<sub>3</sub> or Sb<sub>2</sub>O<sub>3</sub> have smaller crystallite sizes than that of the undoped material. The crystallite sizes were less than 30nm while the calcination temperatures were up to 1050 °C. Grain growth was significantly inhibited by the Sb doping. Measurements of electrical property for the doped sensors showed higher sensitivity to CO at 350 °C than the pure SnO<sub>2</sub> sensor. Among these doping oxide sensors, Er<sub>2</sub>O<sub>3</sub> doped sensor had the highest sensitivity to CO gas.

**KEY WORDS** rare earth oxide, nanocrystalline, sensor

## 1. Introduction

Tin dioxide (SnO<sub>2</sub>) based gas sensors exhibit high sensitivity to various reducing/oxidizing gases. Considerable attention has recently been focused on the development of solid state gas sensors based on films with crystallite size smaller than Debye length of electrons in the material, which showed an increased gas sensitivity and short response time [1~4]. In general, the factors that affect the crystallite size of the SnO<sub>2</sub> based gas sensor materials are fabrication methods, heat treatment conditions and compositions. Doping is an effective way to control the crystallite size. By using suitable dopants, such as Pd, Pt, Al<sub>2</sub>O<sub>3</sub>, CuO, Sb<sub>2</sub>O<sub>3</sub>, MgO, and SiO<sub>2</sub>, the sensitivity and selectivity of a sensor could be remarkably improved [2,5~10]. The additives improved the gas sensitivity and selectivity of a sensor in two ways: either to limit the grain growth, or to reduce the intrinsic Debye length. Studies indicated that if trivalent ions were doped partially into the SnO<sub>2</sub>, the electrical carrier concentration would decrease, so that the Debye length of SnO<sub>2</sub> would increase. On the contrary, pentavalent dopants would bring about a smaller Debye length, thus reduce the sensitivity [5]. The behavior of different valence doping in SnO<sub>2</sub> matrix was investigated in this paper. The selected dopants were Sb<sub>2</sub>O<sub>3</sub>, Y<sub>2</sub>O<sub>3</sub>, Er<sub>2</sub>O<sub>3</sub> and ZrO<sub>2</sub>.

## 2. Experiment

Tin oxide-based powders were prepared by solution co-precipitation method. The thick films for electrical property measurements were prepared using screen print technique. The measurement of gas sensitivity was carried out in a quartz tube with built-in heater and electrodes. The gas concentration was controlled by a flowmeter. The resistance was measured by using four-point-probe method. The sensitivity of the sensor was defined as  $R_a/R_g$ , where  $R_a$  was the resistance of the sensor in air and  $R_g$  was the resistance during exposure to the testing gas. X-ray diffraction was performed on Rigaku rotating anode diffractometer using Cu  $K_\alpha$  radiation.

## 3. Result and Discussion

### 3.1 Effect of doping on crystallite size

Fig.1 indicated that the powders used in the experiment were crystalline with tetragonal rutile structure in the temperature range from 450 °C to 1050 °C. The peak width became narrow with the increase of temperature, which means the crystallite size became large as temperature increased. Fig.1 also revealed the appearance of cubic yttria peak at 1050 °C. This result showed that the doping limit or solubility of yttria in SnO<sub>2</sub> was less than 3% (mass fraction). In the it was, in general, that the solubility will increase with the increase view of

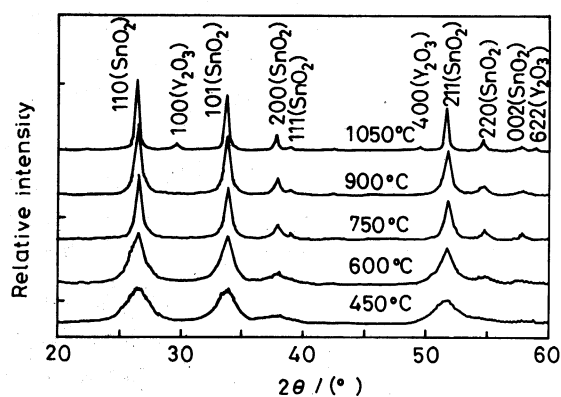


Fig.1 X-ray diffraction patterns of 3% Y-SnO<sub>2</sub> powders calcinated at different temperatures

solid phasediagram, of temperature, and thus the yttria peaks will be supposed to appear at low temperature. The result in Fig.1 seemed in contradiction to that point. In fact, the yttria peaks existed at low temperatures. They became very weak or invisible due to the very fine crystallite size resulted from lower temperature calcination. In order to make sure on peak width change and phase evolution versus temperature, a pellet of this composition was prepared using cold isostatic press method and fired at 1500 °C for 3h. The results showed the intensity of the second phase peak has a big increase and the second phase changed from cubic  $Y_2O_3$  to cubic  $Y_2Sn_2O_7$  (Fig.2). From this point, a way to evaluate the doping limit was provided, i.e., it should check the powder calcinated at high temperature.

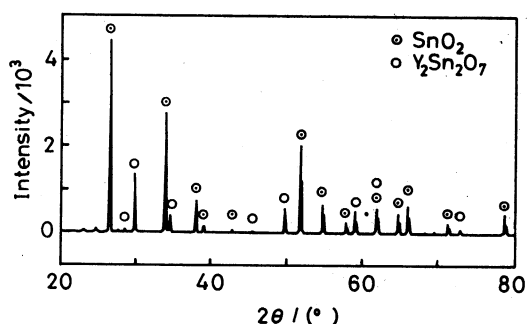


Fig.2 X-ray diffraction patterns of 3% Y-SnO<sub>2</sub> pellet sintered at 1050 °C for 3h

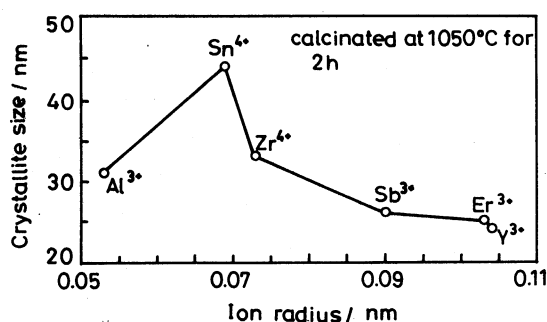


Fig.3 Relationship between SnO<sub>2</sub> crystallite size and ion radii of dopants

The average crystallite size,  $D$ , was estimated by the Debye-Scherrer formula using the full-width-at-half-maximum, which was after the correction for instrumental broadening. From Fig.3, the crystallite size decreases with the increase of  $|r_d - r_{Sn}|$ , here  $r_d$  was the ionic radius of the dopant,  $r_{Sn}$ , the ionic radius of Sn. Y ion had a bigger radius, so it had a smaller solubility in SnO<sub>2</sub> lattice, and the excess content simply acted as a stabilizer of the SnO<sub>2</sub> crystallites, therefore, Y doped SnO<sub>2</sub> in this studies showed the smallest crystallite size. Here, it is emphasized that the crystallite sizes were the average of compositions of 1%~5% for Y-, Sb- and Zr-SnO<sub>2</sub> (the data for Al doped SnO<sub>2</sub> after reference[5]).

### 3.2 Effect of doping on sensitivity

The effects of additives on the gas sensitivity to CO were examined. The typical relationships between resistance and CO concentration for 3% Er<sub>2</sub>O<sub>3</sub> doped tin dioxide thick film sensor materials were shown in Fig.4. The sensitivity of sensors of different metal oxides was shown in Fig.5, here the sensitivity was defined as  $R_a/R_g$ , where  $R_a$  is the resistance of the sensor in air and  $R_g$  is the resistance during exposure to the test gas. The 3% Er<sub>2</sub>O<sub>3</sub>, Y<sub>2</sub>O<sub>3</sub>, Sb<sub>2</sub>O<sub>3</sub> and ZrO<sub>2</sub>-doped sensors showed increase in sensitivity as compared with pure SnO<sub>2</sub> sensor. With the increase of the CO concentration, the sensitivities of doped sensors increased fast while pure SnO<sub>2</sub> only had a slight increase from  $2 \times 10^{-4}$  to  $7 \times 10^{-4}$  by volume. Among them, the 3% Er<sub>2</sub>O<sub>3</sub>-doped SnO<sub>2</sub> had the highest sensitivity in the whole gas concentration measuring range. At  $7 \times 10^{-4}$ , both Y<sub>2</sub>O<sub>3</sub> and

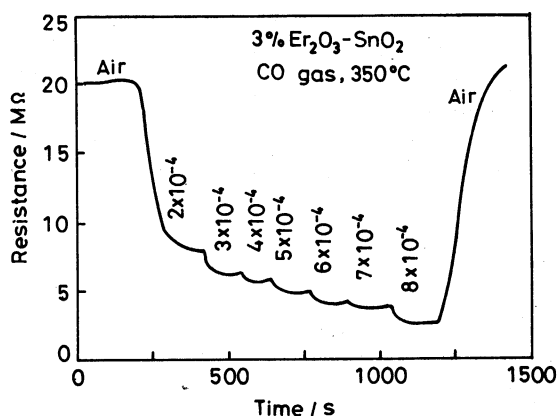


Fig. 4 Resistance vs CO concentration for 3% Er<sub>2</sub>O<sub>3</sub>-SnO<sub>2</sub>

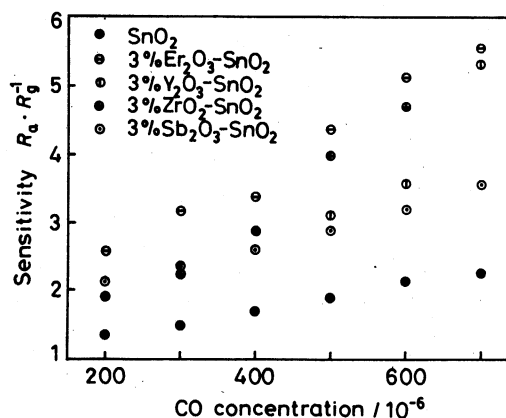


Fig. 5 Sensitivity as a function of CO concentration at 350 °C for various doping materials

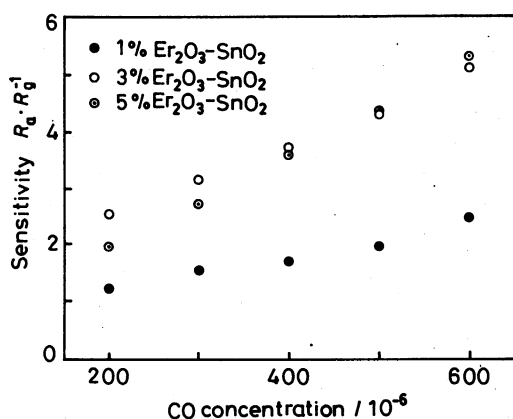


Fig. 6 Sensitivity as a function of different erbium oxide contents in SnO<sub>2</sub> matrix

Er<sub>2</sub>O<sub>3</sub> doped sensors exhibit higher sensitivity values. This may be due to the microstructure changes induced by large ionic radius difference between doped ions and tin ion. Here, the Er ion radius is 0.103 nm, Y ion, 0.104 nm, while Sn ion, 0.069 nm. The difference was over 30%. For the other two doped ions, Zr ion and Sb ion, the difference was less than 30%. It was emphasized that all the sensors used in experiments (pure and doped) have similar crystallite size, therefore the difference in sensitivity might be chiefly due to the difference between ion radius. In addition, the special electronic structure of rare earth ions also plays a part role on the sensitivity. The electronic interaction of SnO<sub>2</sub>

associated with the 4f electrons in Er ion may induce a shift in binding energy of Sn 3d and O1s electrons to a lower energy. The shift will result in the increase of sensitivity<sup>[11]</sup>. However, rare earth ions not only affect the microstructure, but also affect the Debye length. Different contents of rare earth ion doping were checked. Fig. 6 showed the gas sensitivity as a function of erbium oxide content in tin dioxide matrix, this study demonstrated that doping with 3%~5 % has the strong contribution to sensitivity.

#### 4. Conclusions

The additions of yttrium and antimony oxides in tin dioxide by solution coprecipitation

method can limit the grain growth, especially at higher calcination temperatures. SnO<sub>2</sub> doped with 3% Y<sub>2</sub>O<sub>3</sub>, Er<sub>2</sub>O<sub>3</sub>, ZrO<sub>2</sub> and Sb<sub>2</sub>O<sub>3</sub> have higher sensitivity to CO at 350 °C than the pure SnO<sub>2</sub>. Among these doping oxide sensors, Er<sub>2</sub>O<sub>3</sub> doped sensor has the highest sensitivity to CO.

Acknowledgement: This work was supported by the College of Engineering, the University of Michigan, Ann Arbor.

## References

- 1 T.Seyama, A.Kato, K.Fujiishi, M.Nagatani, *Anual. Chem.*, **34**, 1052(1962)
- 2 W.Gopel, K.D.Schierbaum, *Sensors and Actuators B*, **26-27**, 1(1995)
- 3 H.Ogawa, M.Nishikawa, A.Abe, *J.Appl.Phys.*, **53**, 4448(1982)
- 4 C.Xu, J.Tamaki, N.Miura, N.Yamazoe, *J.Electrochem.Soc., Jpn.*, **58**, 1143(1990)
- 5 C.Xu, J.Tamaki, N.Miura, N.Yamazoe, *Sensors and Actuators B*, **3**, 147(1991)
- 6 I.Sayago, J.Gutierrez, L.Ares, J.I.Robla, M.C.Horrillo, J.Getino, J.Rino, J.A.Agapito, *Sensors and Actuators B*, **26-27**, 19(1995)
- 7 M.Schweizer-Berberich, J.G.Zheng, U.Weimar, W.Gopel, N.Barsan, E.Pentia, A.Tomescu, *Sensors and Actuators B*, **31(7)**, 1(1996)
- 8 H.W.Cheong, J.J.Choi, H.P.Kim, J.M.Kim, J.Kim, G.S.Churn, *Sensors and Actuators B*, **9**, 227(1992)
- 9 M.Labeau, U.Schatz, G.Delabouglise, J.Roman, M.Vallet-Regi, A.Gaskov, *Sensors and Actuators B*, **26-27**, 49(1995)
- 10 T.Ratcheva, I.Stambolova, K.Konstantinov, *Sensors and Actuators B*, **21**, 199(1994)
- 11 N.Yamazoe, *Sensors and Actuators B*, **5**, 7(1991)